JOINT EUROPEAN TORUS

JET–P(92)64

D. Naujoks, R. Behrisch, J.P. Coad, L. de Kock
and JET Team

Material Transport by Erosion and Redeposition on Surface Probes in the Scrape-Off Layer of JET

Material Transport by Erosion and Redeposition on Surface Probes in the Scrape-Off Layer of JET

D. Naujoks[1], R. Behrisch[1], J.P. Coad, L. de Kock
and JET Team*

JET-Joint Undertaking, Culham Science Centre, OX14 3DB, Abingdon, UK

[1]Max-Planck-Institut fiir Plasmaphysik, Garching bei Mtinchen, Germany
** See Annex*

Preprint of Paper to be submitted for publication in
Nuclear Fusion

Material Transport by Erosion and Redeposition on Surface Probes in the Scrape-off Layer of JET

D. Naujoks*, R. Behrisch*, J.P. Coad, L. de Kock

JET Joint Undertaking, Abingdon, Oxon OX14 3EA, United Kingdom
*Max-Planck-Institut für Plasmaphysik,
D-8046 Garching bei München, Germany

Abstract

The material transport by erosion and redeposition at the plasma facing wall areas in high temperature plasma experiments has been studied using limiter like carbon probes with well defined surface deposits and depth markers. The probes have been exposed in the scrape-off layer (SOL) of the Joint European Torus (JET) during single discharges. For the evaluation of these experiments a computer program ERO has been developed. The calculated erosion/deposition rates for carbon as a function of the distance to the last closed flux surface (LCFS) agree well with the experimental results. For a single ^{4}He JET discharge erosion yields of 530 Å for the Si deposit and 80 Å for V have been measured near the LCFS. A large amount of redeposited Si (about 17% of the sputtered atoms) has been found on the probe surface in co-deposition with carbon on an area not favourable by the proposed model. This observation can be explained by an additional force on the impurity ions (for example the existence of a local electric field) which may cause the deposition.

1. Introduction

At surfaces exposed to a magnetically confined hot plasma erosion and redeposition has been observed [1-6]. This erosion and redeposition has also been studied with computer simulation programmes [2,3,7-9]. In these models neutral atoms are sputtered from the plasma exposed surface and are ionized upon entering the plasma. The ions are guided along and may diffuse perpendicular to the magnetic field lines. They move away from the source or they return to the areas where the magnetic field lines intersect the surface, such as at the sides of limiters or at divertor plates. Upon impinging on the solid surface the ions may be deposited or backscattered and they may also cause further sputtering. The erosion/redeposition processes depend largely on the local plasma temperature and the magnetic field geometry. At the divertor

plates the magnetic field lines intersect at a small angle in the toroidal direction. Therefore the toroidal transport is favoured compared to the poloidal transport and for a divertor with toroidal symmetry such as ITER the net erosion is predicted to be largely reduced due to the redeposition of eroded atoms at the very area of erosion [7,8]. In order to quantitatively understand this material transport by erosion and redeposition at the plasma exposed wall areas in fusion devices, limiter like carbon probes have been inserted in the SOL of JET and have been exposed to single discharges. We have chosen a carbon test sample with a depth marker to measure erosion/deposition of the carbon. In addition we have evaporated onto the carbon probe two dots of materials which have different ionization lengths to explore details of the transport. The results of the experiments and a model to describe the process of erosion and redeposition are presented in the following.

2. The Model for Erosion and Redeposition

A solid probe with surface area $L_x * L_y$ may be exposed in the SOL of a magnetically confined plasma containing various ion species 'i', such as $D^+, He^+, He^{2+}, O^+, O^{2+} \ldots, C^+, C^{2+}, C^{3+} \ldots$ (see fig.1). Due to bombardment from the plasma the surface layer concentration of each element 'I' is changed by sputter erosion and redeposition. This change of the surface concentrations of each element 'I' (i.e. C,Si,V ...), $\partial n_s^I(x,y,t)/\partial t$ [$cm^{-2}s^{-1}$], at the point (x,y) with time t is given by [9]:

$$\frac{\partial n_s^I(x,y,t)}{\partial t} = \Gamma^I(x,y,t)\ (1-R_n^I) - \sum_i \Gamma^i(x,y,t)\ Y_{i,I}(E_o,\Omega_o,n_s^I(x,y,t)) +$$

$$+ \int_0^{L_x}\int_0^{L_y} \frac{dx'dy'}{\Delta S} \sum_i \int_E \int_\Omega \int_0^\infty \frac{1}{\lambda_{iz}^I(r)} \exp\left[-\int_0^r dr'/\lambda_{iz}^I(r')\right]\ \Gamma^i(x',y',t) \cdot$$

$$\cdot \frac{\partial^2 Y_{i,I}}{\partial\Omega\ \partial E}\ (E_o,\Omega_o,n_s^I(x',y',t);E,\Omega,)\ dr\ dE\ d\Omega, \qquad (1)$$

Here $\Gamma^i(x,y,t)$ are the plasma ion flux densities of species 'i' to the probe surface and R_n^i are the particle reflection coefficients; $Y_{i,I}(E_o,\Omega_o,n_s^I)$ are the sputtering yields of probe

element 'I' under bombardment with ion species 'i'; $\partial^2 Y_{i,I}/\partial\Omega\ \partial E$ represents the energy and angular distributions of sputtered particles 'I', which depend on the incident energy E_o and the angle of incidence $\Omega_o=(\theta_o,\phi_o)$ of the ions, and $\Delta S=dxdy$ denotes the deposited surface area. The term

$$\frac{1}{\lambda^I_{iz}(r)}\ \exp\left[-\int_0^r dr'/\lambda^I_{iz}(r')\right]dr \qquad (2)$$

is the probability for the sputtered atoms moving along the direction $\Omega=(\theta,\phi)$ to be ionized in the interval $[r,r+dr]$ (fig.1). The distance R from the point of sputtering (x',y') to the point of deposition (x,y) is determined by the flight path before ionization r, the angle θ, the azimuthal angle ϕ and by the angle α between the surface of the probe and the magnetic field lines:

$$r = R\left[\tan^2\alpha/(\sin^2\theta\ \tan^2\alpha + \cos^2\theta + \sin(2\theta)\ \cos\phi\ \tan\alpha)\right]^{1/2}, \quad (3)$$

with $R = ((x'-x)^2+(y'-y)^2)^{1/2}$. The mean ionization length

$$\lambda^I_{iz}(r,E,T_e) = (2E/m_I)^{1/2}/(n_e(r_{LCFS}(x',r))*<\sigma v>)$$

with m_I being the mass of ions 'I', depends on the local plasma parameters and the velocity $(2E/m_I)^{1/2}$ of the sputtered atoms. The rate coefficients for electron impact ionization $<\sigma v>$ can be calculated as a function of the local plasma temperature T_e by the convenient approximate formulae proposed in [10]. The distance to the LCFS is:

$$r_{LCFS}(x',r,t) = z_o(t)+(L_x-x')\sin\alpha\ -r(\cos\theta\ \cos\alpha + \sin\theta\ \sin\alpha\ \cos\phi).$$

The first term on the right hand side of equ. (1) describes the deposition of impurity ions 'I' on the surface with the sticking probability of $(1-R^I_n)$. The sputtering of probe atoms 'I' by the incoming flux of all ion species 'i' is represented by the second term. The third term on the right hand side of equ. (1) describes the redeposition of atoms which had been sputtered, ionized in the plasma and returning back to the probe surface. The sputtering yields for the different species 'I' are proportional to the actual surface concentrations $n^I_s(x,y,t)$. The plasma temperature and density in the SOL are assumed to decrease exponentially with distance to the LCFS.

$$n_e(x,t) = n_e^{LCFS}(t)*\exp(-(z_o(t)+(L_x-x)*\sin\alpha)/\lambda_\Gamma), \quad (4)$$

$$T_e(x,t) = T_e^{LCFS}(t)*\exp(-(z_o(t)+(L_x-x)*\sin\alpha)/\lambda_T), \quad (5)$$

with n_e^{LCFS} being the electron density and T_e^{LCFS} the electron temperature at the LCFS. λ_Γ and λ_T denote the density and temperature e-folding lengths, respectively. The total fluxes of ions from the plasma to the probe area are given by [2]:

$$\Gamma^i(x,y,t) = 0.5\ f_i\ n_e(x,t)\ c_s(x)\ \sin(\alpha) \quad (6)$$

where $c_s(x)=((T_i(x)+T_e(x))/m_p)^{1/2}$ is the ion acoustic speed at the LCFS and m_p is the mass of plasma ions. The concentrations of ion species 'i' in the plasma with respect to the electron density are denoted by f_i (by definition: $\sum f_i*q_i = 1$).

The motion of the sputtered and subsequently ionized atoms is described by the velocity component parallel to the magnetic field $v_\parallel^o$ and in addition by the effect of collisional friction:

$$dv_\parallel/dt = \nu_{coll}*(\ v_{pl} - v_\parallel\ ), \quad (7)$$

where $v_\parallel$ is the velocity of impurity ions parallel to the field lines; v_{pl} is the drift velocity of the plasma ions which is directed toward the probe surface. The collisional frequency can be calculated by [11]:

$$\nu_{coll}=6.81*10^{-14}*(m_p*m_I/(m_p+m_I))^{1/2}*\frac{Z_p^2Z_I^2*\ln\Lambda*n_e[m^{-3}]}{m_I*(kT_e[eV])^{3/2}}\ [s^{-1}] \quad (8)$$

with Z_p and Z_I being the charge numbers of plasma and impurity ions, respectively, and $\ln\Lambda$ the Coulomb logarithm [11].

It was assumed that the sputtered atoms are neutrals and move on straight trajectories without collisions along their sputtered direction until they are ionized in the plasma. After ionization they precess around the magnetic field direction whilst retaining their initial parallel velocity $v_\parallel^o=-(2E/m_I)^{1/2}\cos\delta$ (fig.1.). Those ions moving away from the probe surface ($\delta<90^\circ$, fig.1) will be slowed down by the plasma flow and they may be finally accelerated towards the probe surface. Equ. (7) also allows calculation of the time of flight τ until the impurity ions reach the surface. This time of flight determines the ionization state q near the surface which determines the energy of the ions impinging on the surface according to

$$E_o = m_I v_\parallel^2/2 + 3kT_e q. \quad (9)$$

The effect of cross field transport is taken into account by introducing a coefficient $D_\perp$ which means that an impurity ion diffuses a distance $(D_\perp \tau)^{1/2}$ in a time τ.

3. Experimental

Three surface probes have been exposed during single discharges in the SOL in the shadow of the limiter using the Fast Transfer System (FTS) (fig.2). The target holder was a 45 mm diameter cylinder of POCO graphite which allows exchange of the exposed carbon strips. The surface of the C strips (10x37 mm^2) which were analysed had been implanted with a depth marker of Er atoms at a depth of about 2800 Å in order to measure the net erosion/redeposition of carbon. Additionally, surface deposits of Si and V were evaporated locally on dots of 3 mm diameter. Redeposition profiles of these elements should give information about the effects of $\parallel$ and $\perp$ transport in the SOL and resulting from the differences in the ionization length.

Each of the three probes has been exposed during a full discharge, i.e. during the current ramp up, the current flat top and the current ramp down phases. The relevant plasma parameters during the dominant phase, i.e. plasma close enough to give a dominant fluence for these discharges, are given in Table 1.

1. discharge number	#25893	#25970	#27740
2. probe number	1	2	3
3. filling gas	D	D	He^4
4. plasma current	3 MA	3 MA	3 MA
5. volume average density $\bar{n}_e$	3.10^{-19} cm^{-3}	3.10^{-19} cm^{-3}	3.10^{-19} cm
6. magnetic field	2.8 T	2.8 T	3.3 T
7. power input	7.8 MW NBI	7.8 MW NBI	3 MW NBI + 1 MW ICRH

Table 1: Plasma Parameters

The probes have been inserted with the FTS which enters the torus horizontally at an angle of 25° with respect to the radius into the torus (fig.2.). The probes were subsequently rotated by an angle of 15° in order to adjust the exposed surface of the carbon strips in the direction of the magnetic field lines during

the plasma discharges. The position of the probes is shown in fig.2b. An inclination angle of $\alpha = 10^{o}$ between the probe surface and the magnetic surface was chosen for all three probes. Before and after exposure the surface layers of the carbon strips were analyzed using ion beam methods (RBS, PIXE and nuclear reactions) at the 2.5 MeV accelerator at the Max-Planck Institut für Plasmaphysik, Garching. The amount of deposited D, O, and erosion/redeposition of C, Si and V was determined quantitatively.

4. Results

The erosion/deposition behaviour for the materials on the probe surface depends on the electron density and temperature profiles in front of the exposed probe and on the impurity concentrations, such as C and O, in the SOL [3,4]. These quantities have not been measured simultaneously in the discharges to which the probes were exposed. Therefore typical values for the JET scrape-off layer [12-14] have been used in the computer calculation. The carbon ion concentration in the SOL is typically from 10% [5] up to 25% [15] of the plasma ions. Oxygen is normally present at the ≈ 1% level [16]. For the charge states average values are taken from the literature [16,17]. All these assumptions introduce uncertainties in the computer calculation. In the end the values chosen are those which are consistent with the values measured in previous JET discharges and which gave the best agreement between the calculated and the measured values. The input parameters which are used in the calculations are summarized in table 2.

For solving equ. (1) a computer programme named ERO has been developed. A first-order accuracy difference method in respect to time in which for each time step numerical integration methods are applied.

1. discharge number	#25893	#25970	#27740
2. probe number	1	2	3
3. n_e^{LCFS} [cm^{-3}], electron density at the LCFS,	$1*10^{13}$	$1*10^{13}$	$1*10^{13}$
4. T^{LCFS} [eV], electron temperature at the LCFS	30	30	30
5. λ_Γ [mm], density e-folding length,	15	15	15
6. λ_T [mm], temperature e-folding length,	40	40	40
7. filling gas	D	D	He
8. q, charge states:			
carbon	4	4	4
oxygen	6	6	6
9. f_i, concentrations in the SOL:			
f_{D^+}	0.58	0.58	0.01
f_{He^+}	0	0	0.05
$f_{He^{2+}}$	0	0	0.26
$f_{C^{4+}}$	0.09	0.09	0.09
$f_{O^{6+}}$	0.01	0.01	0.01
10. z_o [mm], distance of the probe tip to the LCFS	25	7	4
11. t [s], time of exposure	10	10	8

Table 2: Parameters used in the calculations

With the parameters given in Table 2 for the D discharges (#25983, probe 1 and #25970, probe 2) the dependence of carbon net erosion/deposition at the area $x=L_x$ as a function of the distance z_o of the probe tip from the LCFS was calculated and is shown in fig.3. Only physical sputtering was considered and the distributions of sputtered particles were calculated by the TRIM type Monte Carlo program IIAM [18] with average angles of incidence taken from [19]. The experimentally obtained values at the probe tip ($x=L_x$) for discharges #25893 and #25970 are also indicated. At larger distances from the LCFS the plasma densities are low. The resulting mean ionization lengths of sputtered carbon atoms are large. The atoms are mostly ionized deeper in the SOL and cannot be redeposited on the probe. The deposition found for

distances of probe tip to the LCFS z_o>10 mm are due to carbon ions present in the SOL. These ions originate from other wall areas and this carbon deposition allows a determination of the carbon concentration in the SOL. Redeposition of locally eroded carbon atoms gives a contribution to the deposition only if the ionization length is short, i.e. if the probe is close to the LCFS (fig.1).

For probe 1 exposed during discharge #25893 at an average distance of z_o=25 mm a nearly uniform D deposition of about $1*10^{17}$ D/cm^{-2} was measured. This is in agreement with the measured carbon deposition (fig.3) of about 200 Å if we assume a ratio of D:C=0.44, which is close to saturation [5].

For probe 3 which was exposed to discharge #27740 at the distance of z_o=4 mm the calculated carbon net erosion/deposition along the exposed area is shown in fig.4a together with the experimentally obtained values. For position x>5 mm the measured and calculated values agree within the experimental errors. The net erosion is nearly uniform along the probe. Because of the small inclination angle $\alpha=10^\circ$ of the probe the plasma parameters in front of the probe surface have only a small variation. No carbon erosion was found at the areas where the carbon was covered with the Si and V deposits.

The large amount of carbon deposited on the area x<5 mm cannot be explained by carbon transport along the probe, neither by a carbon concentration profile in the SOL as predicted by (6). This deposit may be the result of a local C source such as at the side of the probe being exposed perpendicular to the plasma flux:

- Physically sputtered carbon atoms with a kinetic energy of several eV from the side cannot be the cause of the strong deposition on x<5 (fig.5) because of the larger ionization lengths of sputtered atoms, which lead to a much broader distribution.

- The measured peaked distribution of deposited carbon is probably caused by a thermal carbon source. The flux of plasma ions toward this area, where $\alpha\cong 90^\circ$, is increased by a factor of $\sin(90^\circ)/\sin(10^\circ)=5.8$ compared to the flux onto the probe surface (see equ.6). The maximum surface temperature T_s at the side wall at the end of the discharge can be roughly estimated by [20]:

$$T_s = T_o + 2*P*\sqrt{t/(\pi\rho ck)} \qquad (10)$$

where T_o is the starting temperature being about 300-400 K for JET. P is the heat flux density: $P=0.5*\gamma*kT_e*n_e*c_s$ [21], t is the discharge time, and for carbon the physical parameter $2/(\pi\rho ck)^{1/2}=0.9$ cm^2 K $W^{-1}s^{1/2}$ [14]. With the energy transmission factor $\gamma=8$ we obtain $P\cong$ 500 [W/cm^2], which would result in about $T_s=1700$ K at the end of the discharge.

The amount of atoms released by thermal sublimation during such a heat pulse is only about 10^{10} atoms/cm^2 [20]. This is far too small to explain the observed C deposition profile.

- The temperature is however well above 1200 K where Radiation Enhanced Sublimation (RES) is observed in laboratory experiments. To get an estimate of the erosion two average temperatures, i.e. Ts=1200 K and Ts=1600 K, have been taken at the side of the target holder during the discharge. The sputtering yields by RES for these temperatures have been taken from [22]. The carbon atoms released by RES become ionized near the edge in the SOL plasma and might thus be redeposited on the probe surface. The results of the calculations are introduced in Fig.4a.

The depositions of deuterium and oxygen on probe 3 are shown in fig.4b (y=4). On the areas where the markers had been deposited, i.e. x=7-10 mm for Si and x=20-23 mm for V the concentrations of deuterium have a minimum, while the concentration of oxygen shows a small local maximum. This is consistent with the observation that no carbon deposition has been measured at these areas (fig. 4.a), i.e. D trapping by co-deposition with carbon is insignificant on the Si and V. The largest amount of both D and O has been found on position x=0-5 mm which can be explained by co-deposition with carbon (see also fig. 4a).

Fig.4c shows the amount of Si and V on probe 3 which was measured before and after exposure to discharge No. 27740. Si and V had been evaporated at the positions x=7-10 mm and x=20-23 mm, respectively. The measured erosion is about 530 Å for Si (corresponding to 90% of the deposit) and 80 Å for V. Redeposited Si is only observed on the area x<5, where it was probably co-deposited with carbon (fig.4a,4c,5a). The amount of Si measured on other areas of the probe is in the noise level of the analysis techniques. Redeposited V was not found on the probe. As was explained in [9] redeposited impurity atoms can only be found on

deposition dominant areas where they are permanently trapped such as by co-deposition with carbon. If the impurity ions which were sputtered and ionized impinge on erosion dominant areas (a process of several micro seconds) they will be sputtered again and so transported further until they leave the probe surface into the SOL. They will eventually be deposited on other deposition dominant areas such as the vessel walls.

Fig. 5a shows the distribution of Si on probe 3 after exposure to discharge #27740. The initial Si deposit around position x=9 mm is reduced by a factor of about 9 (fig. 4c), whilst the observed redeposition of Si atoms at the area of the probe surface furthest from the LCFS is about 17% of the sputtered Si (fig.5a). As mentioned above, some Si may be trapped in this region by co-deposition, but this large absolute amount is unexpected. In the model described in section 2 (see also [7,8]) the favourable direction of transport is toward the end of the probe ($x \leq L_x$). Less than 1% of the Si is sputtered in the direction away from the LCFS, i.e. $\theta < 10^\circ$, $\pi/2 < \phi < 3*\pi/2$ (fig.1,2), and only this Si can be redeposited on the "false" end of the probe (fig.5b).

Virtually no deposition is found in the direction toward smaller distances to the LCFS. The calculations predict transport in this direction, but the redeposited Si is quickly removed again by sputtering and thus effectively transported along the probe surface into the SOL in agreement with the experiment.

The Calculated distributions of Si along the center line of the strip (y=4) for several situations are shown in fig.6. By increasing the cross field diffusion coefficient $D_\perp$ to a value of about 4 m^2/s the amount of redeposited Si expected on x<5 mm increases. By further increasing $D_\perp$ the distribution becomes broader and consequently the number of Si atoms redeposited along the center line decreases (not shown in fig.6).

The relatively large fraction of redeposited Si and deposited C which was measured at x≤5 mm with the maximum deposition at x≈0 mm (fig. 4a, 5a) could also be explained if we assume the existence of an electric field in the SOL which attracts the impurity ions onto the probe surface. First estimations show that a value of about 60 V/cm for the electric field E would be needed to describe the peaked deposition on the probe edge. Such a

potential could be sustained perpendicular to the magnetic surfaces in the Sol-region due to the inhomogeneity of the temperature profile.

The calculated erosion of the Si deposit agrees quite well with the measured value (fig.6) but for the V deposit an erosion of about 440 Å was calculated which differs largely from the experimentally measured value of 80 Å (fig.6). One possible explanation is the influence of oxygen and carbon on the surface binding energy. This leads to a decrease of the sputtering yields for several metals [23].

5. Conclusions

The experiments described here present a powerful tool to investigate the transport of impurities in the SOL near limiters and on divertor plates. The implanted depth markers show the net erosion/deposition of the bulk material, while the evaporated dots of selected elements, in this case Si and V, show how these elements are transported parallel and perpendicular in the local plasma. Experiments, such as these, are an important step to verify the results of calculations about erosion and deposition dominant areas on a probe surface and in the validation of the models describing the reduction of erosion by immediate local redeposition such as predicted by some computer code calculations [2,7,8].

In the experiments a relatively large deposition was measured in the direction not expected from the models [2,7,8]. In order to explain this deposition an additional attractive force, such as an electric field, had to be assumed. The lack of deposition at the areas in the direction of expected material transport is probably due to repetitive re-erosion, so that the material ends up in the SOL plasma. As was shown in section 4 for the erosion of V even the "simple" physical sputtering which is quite well understood under laboratory conditions and with computer simulation is not reproduced in plasma experiments.

The theoretical model (section 2) is a first attempt to describe the plasma-surface interaction for a magnetically confined plasma in a simple manner and has to be improved. It is shown both in experiment and calculation that the distribution of redeposited material is widely spread which is caused by the broad

energy and angular distributions of sputtered atoms, their ionization lengths and the magnetic field geometry.

The present investigations have been performed for toroidal and poloidal material transport at a poloidal limiter. In order to solve the important question about erosion and redeposition on the divertor plates in a future fusion device, such as ITER, experiments and calculation for this geometry are needed. The experiments should be performed exposing the probes using single discharges or during a fraction of single discharges with the detailed knowledge about the plasma parameters (electron density and temperature profiles, impurity concentration) in the SOL.

Acknowledgements
It is our great pleasure to thank Dr. A. Poolman and Drs. E. Snoeks for the generous support in providing the marker implantantion performed at the FOM Institute for Atomic and Molecular Physics, Amsterdam. These experiments have been actively supported by Prof. Dr. K. Pinkau. The samples used in this experiments have been prepared Mrs. G. Haag, G. Mühlbauer, J. Perchermeier and H. Kukral. The excellent technical help by G. Kavaney in performing the experiments with the FTS at JET is also greatly acknowledged. Dr. J. Igitkhanov and Dr. W. Feneberg contributed with several helpful discussions.

REFERENCES:

[1] COAD, J.P., BEHRISCH, R, ROTH, J, et al., Proc. 14th Europ. Conf. on Contr. Fusion and Plasma Phys., Madrid, (1987) 744.

[2] McCRACKEN, G.M., EHRENBERG, J., STOTT., P., et al., J. Nucl. Mater. **145-147** (1987) 621.

[3] McCRACKEN, G.M., STANGEBY, P.C., GOODALL, D.H.J., et al., Fusion Technology (1988) 151.

[3] BEHRISCH, R., EHRENBERG, J, J. Nucl. Mater. **155-157** (1988) 95.

[4] McCRACKEN, G.M., GOODALL, D.H.J., STANGEBY, P.C., et al., J. Nucl. Mater. **162-164** (1989) 356.

[5] BEHRISCH, R., COAD, J.P., EHRENBERG, J., et al., J. Nucl. Mater. **162-164** (1989) 598.

[6] EHRENBERG, J., McCRACKEN, G.M., BEHRISCH, R., et al.

[7] HARRISON, M.F.A., HOTSTON, E.S., J. Nucl. Mater. **176&177** (1990) 256.

[8] BROOKS, J.N., Fusion Technology **18** (1990) 239.

[9] NAUJOKS, D., BEHRISCH, R., in Controlled Fusion and Plasma

Physics (Proc. 19th Int. Conf. Innsbruck, 1992) Vol.2 (1992) 843.

[10] LENNON, M.A., BELL, K.L., GILBODY, H.B., et al., Culham Laboratory, Rep. CLM-R270 (1986).

[11] BROOKS, J.N., PETRAVIC, M., KUO-PETRAVIC, G., Contrib. Plasma Physics **28** (1988) 4/5, 465.

[12] ERENTS, S.K., TAGLE, J.A., McCRACKEN, G.M., et al., NUCLEAR FUSION **26** (1986) 1591.

[13] ERENTS, S.K., TAGLE, J.A., McCRACKEN, G.M., et al., NUCLEAR FUSION **28** (1988) 1209.

[14] ERENTS, S.K., TAGLE, J.A., McCRACKEN, G.M., et al., J. Nucl. Mater. **162-164** (1989) 226.

[15] BERGSÅKER, H., COAD, J.P., BEHRISCH, R., et al., J. Nucl. Mater. **176&177** (1990) 941.

[16] MATTHEWS, G.F., J. Nucl. Mater. **162-164** (1989) 38.

[17] STANGEBY, P.C., J. Phys.D: Appl. Phys. **20** (1987) 1472.

[18] Afanas'ev, V.P., Naujoks, D., Manukhin, V.V., et al., Simulation of Particle Interactions with Surfaces, MEI Press, Moscow (1992) (in Russian).

[19] DeWALD, A.B., BAILEY, A.W., BROOKS, J.N., Phys. Fluids **30**(1) (1987) 267.

[20] BEHRISCH, R., J. Nucl. Mater. **93&94** (1980) 498.

[21] STANGEBY, P.C., J. Nucl. Mater. **145-147** (1987) 105.

[22] ROTH, J., VIETZKE, E., HAASZ, A.A., in Supplement to the Journal NUCLEAR FUSION Vol.1 (1991) 63.

[23] KELLY, R., Nucl. Instr. and Meth. **B18** (1987) 388.

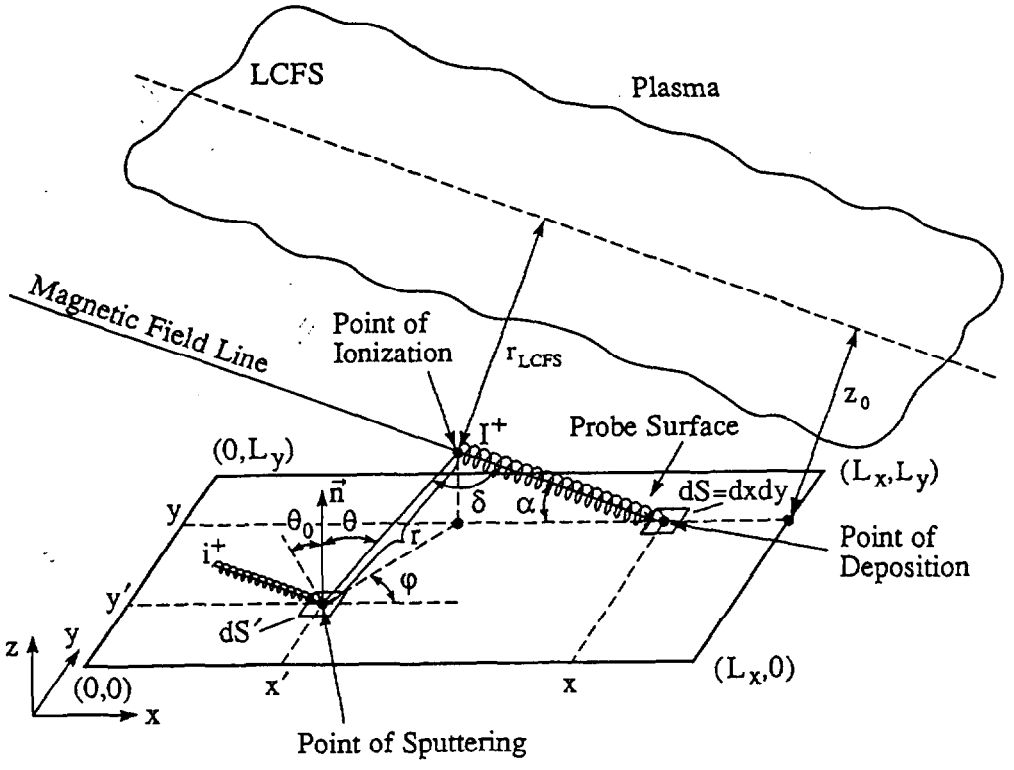

Fig.1 Model geometry

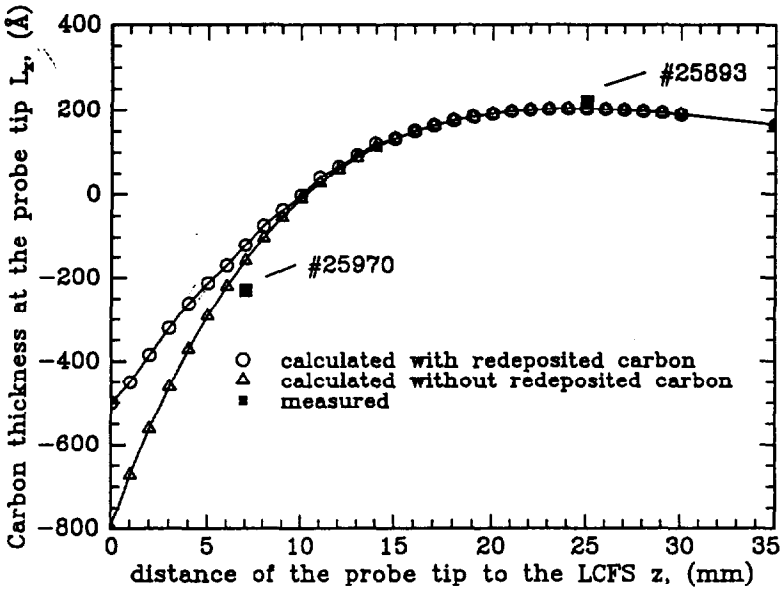

Fig.3 Calculated ero./dep. thickness at a carbon probe in dependence on the distance of the probe tip from the LCFS together with measured values for the discharges #25983 and #25970

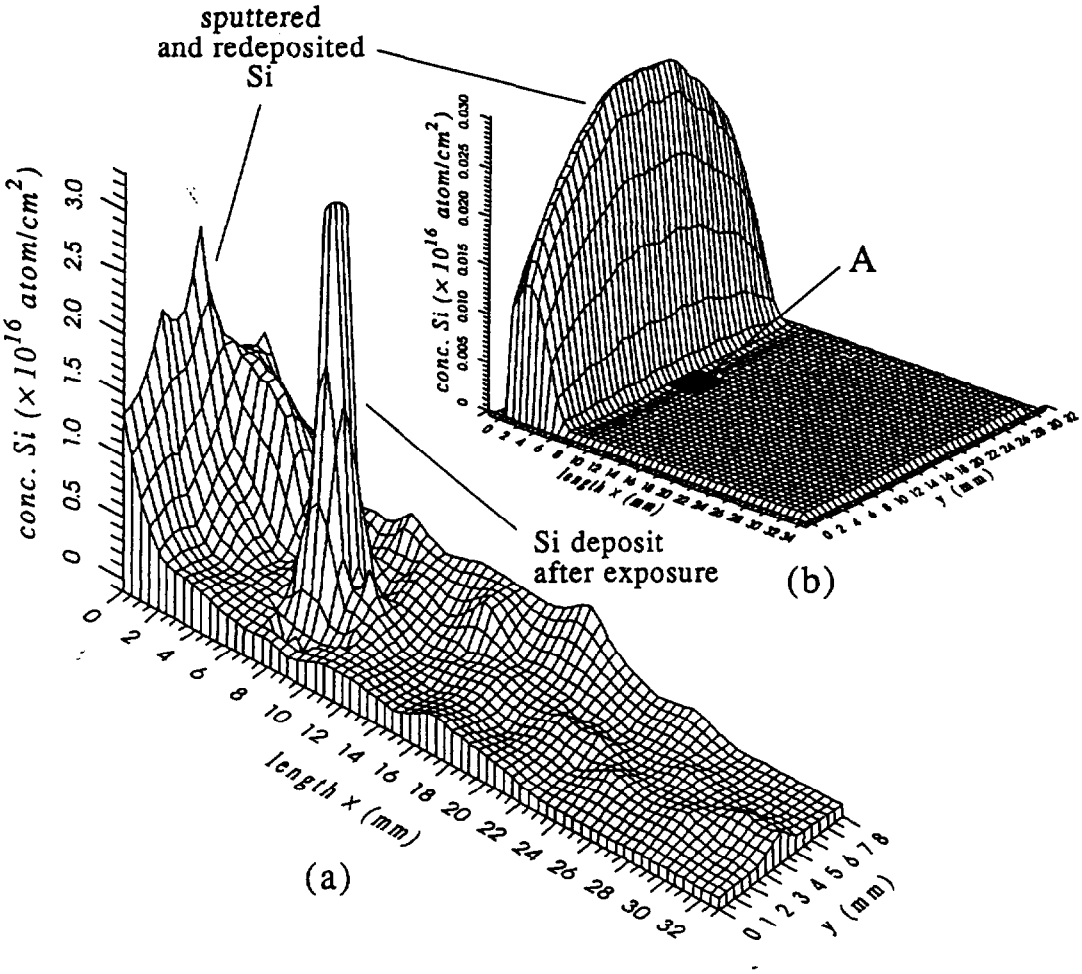

Fig.5 (a) Measured spatial distribution of redeposited Si after exposure to #27740; (b) Calculated distribution for this case with parameters from table 2. The area A indicates the position of the Si deposit before and after exposure. The Si peak on area A is also obtained in calculation but not shown ($D_{\perp}$=1 m^2/s).

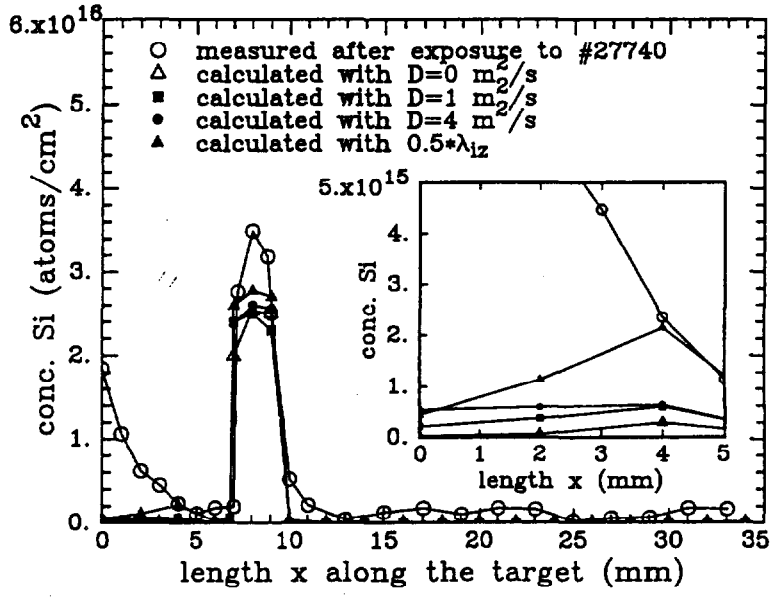

Fig.6 Distribution of redeposited Si along the middline of the carbon strip

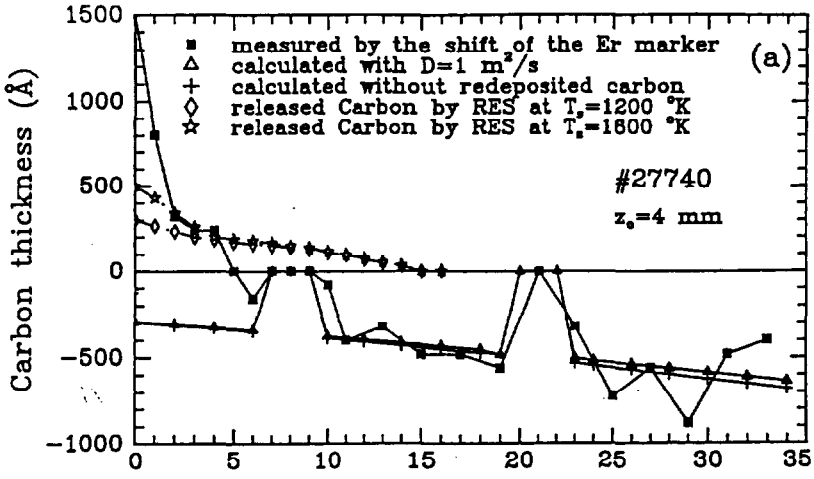

Fig.4a Erosion/deposition of carbon along the probe. The theoretical results are shown in comparision with the measured values

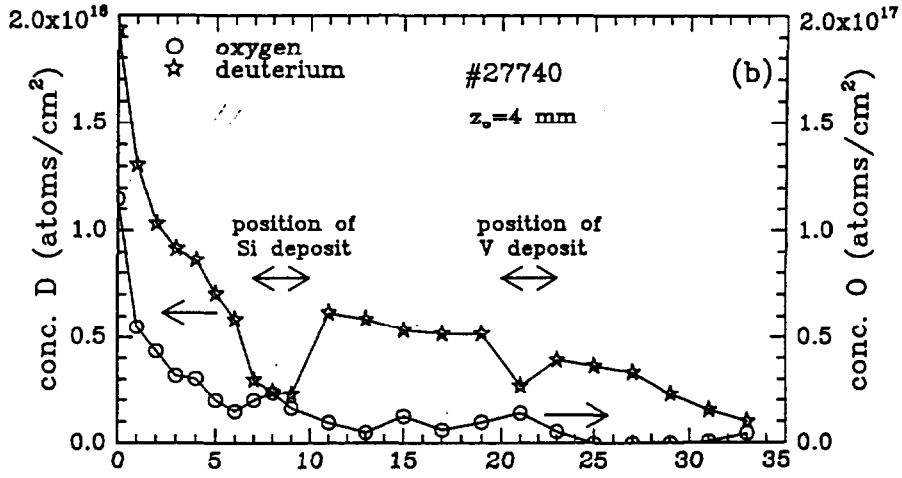

Fig.4b Deposition of deuterium and oxygen on the probe exposed to #27740

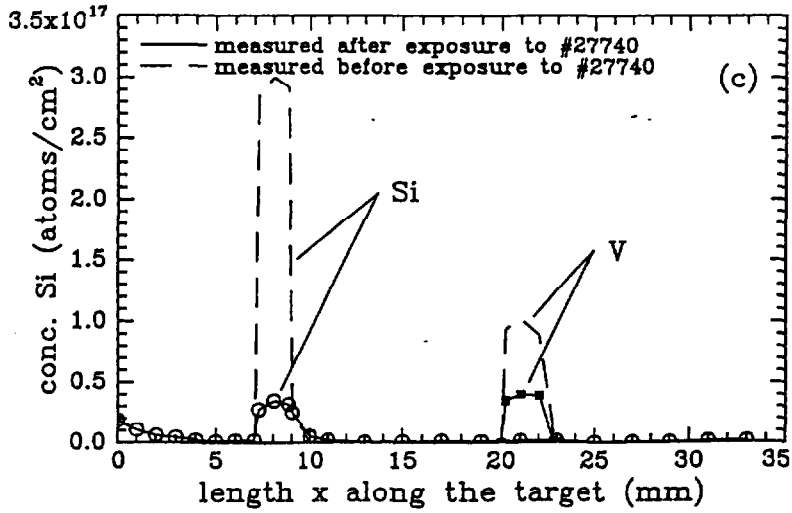

Fig.4c Erosion of the Si and V deposits during discharge #27740

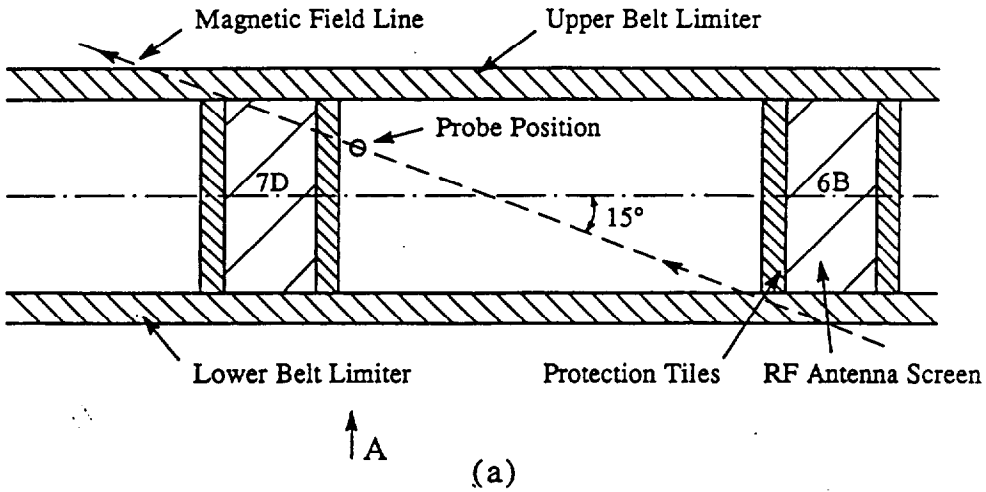

(a)

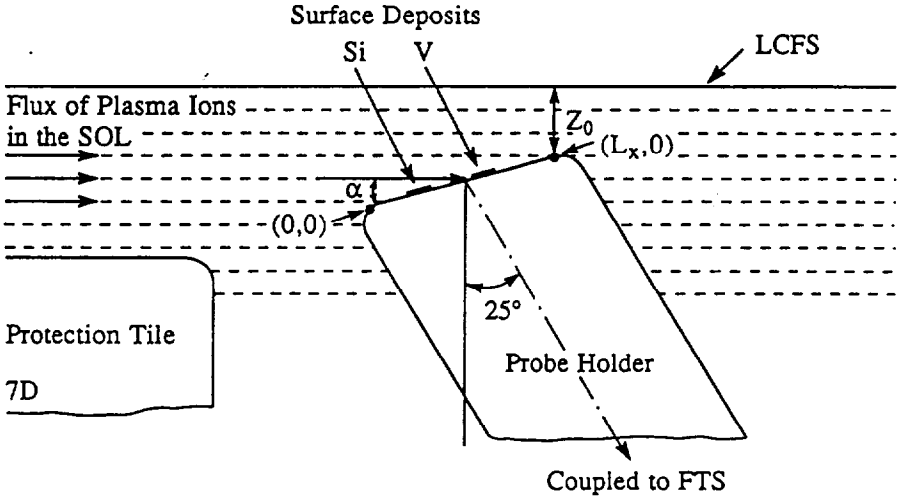

(b)

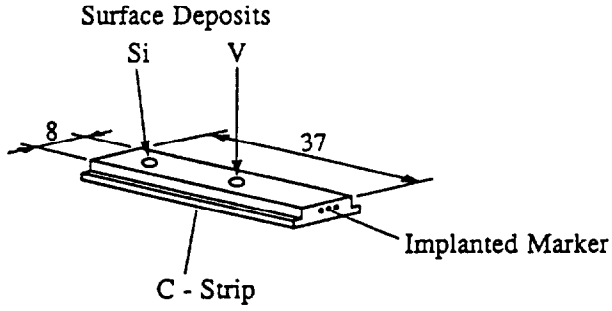

(c)

Fig.2 (a) Position of the surface probe in the SOL of JET. The connection lengths at the electron drift side is 2.1 m and 60m at the ion drift side
(b) Schematic of the probe position relative to the LCFS
(c) Carbon strip with the areas of implantation and the evaporated dots of Si and V

Appendix I

THE JET TEAM

JET Joint Undertaking, Abingdon, Oxon, OX14 3EA, U.K.

J.M. Adams[1], B. Alper, H. Altmann, A. Andersen[14], P. Andrew, S.Ali-Arshad, W. Bailey, B. Balet, P. Barabaschi, Y. Baranov, P. Barker, R. Barnsley[2], M. Baronian, D.V. Bartlett, A.C. Bell, G. Benali, P. Bertoldi, E. Bertolini, V. Bhatnagar, A.J. Bickley, D. Bond, T. Bonicelli, S.J. Booth, G. Bosia, M. Botman, D. Boucher, P. Boucquey, M. Brandon, P. Breger, H. Brelen, W.J. Brewerton, H. Brinkschulte, T. Brown, M. Brusati, T. Budd, M. Bures, P. Burton, T. Businaro, P. Butcher, H. Buttgereit, C. Caldwell-Nichols, D.J. Campbell, D. Campling, P. Card, G. Celentano, C.D. Challis, A.V.Chankin[23], A. Cherubini, D. Chiron, J. Christiansen, P. Chuilon, R. Claesen, S. Clement, E. Clipsham, J.P. Coad, I.H. Coffey[24], A. Colton, M. Comiskey[4], S. Conroy, M. Cooke, S. Cooper, J.G. Cordey, W. Core, G. Corrigan, S. Corti, A.E. Costley, G. Cottrell, M. Cox[7], P. Crawley, O. Da Costa, N. Davies, S.J. Davies[7], H. de Blank, H. de Esch, L. de Kock, E. Deksnis, N. Deliyanakus, G.B. Denne-Hinnov, G. Deschamps, W.J. Dickson[19], K.J. Dietz, A. Dines, S.L. Dmitrenko, M. Dmitrieva[25], J. Dobbing, N. Dolgetta, S.E. Dorling, P.G. Doyle, D.F. Düchs, H. Duquenoy, A. Edwards, J. Ehrenberg, A. Ekedahl, T. Elevant[11], S.K. Erents[7], L.G. Eriksson, H. Fajemirokun[12], H. Falter, J. Freiling[15], C. Froger, P. Froissard, K. Fullard, M. Gadeberg, A. Galetsas, L. Galbiati, D. Gambier, M. Garribba, P. Gaze, R. Giannella, A. Gibson, R.D. Gill, A. Girard, A. Gondhalekar, D. Goodall[7], C. Gormezano, N.A. Gottardi, C. Gowers, B.J. Green, R. Haange, A. Haigh, C.J. Hancock, P.J. Harbour, N.C. Hawkes[7], N.P. Hawkes[1], P. Haynes[7], J.L. Hemmerich, T. Hender[7], J. Hoekzema, L. Horton, J. How, P.J. Howarth[5], M. Huart, T.P. Hughes[4], M. Huguet, F. Hurd, K. Ida[18], B. Ingram, M. Irving, J. Jacquinot, H. Jaeckel, J.F. Jaeger, G. Janeschitz, Z. Jankowicz[22], O.N. Jarvis, F. Jensen, E.M. Jones, L.P.D.F. Jones, T.T.C. Jones, J-F. Junger, F. Junique, A. Kaye, B.E. Keen, M. Keilhacker, W. Kerner, N.J. Kidd, R. Konig, A. Konstantellos, P. Kupschus, R. Lässer, J.R. Last, B. Laundy, L. Lauro-Taroni, K. Lawson[7], M. Lennholm, J.Lingertat[13], R.N. Litunovski, A. Loarte, R. Lobel, P. Lomas, M. Loughlin, C. Lowry, A.C. Maas[15], B. Macklin, C.F. Maggi[16], G. Magyar, V. Marchese, F. Marcus, J. Mart, D. Martin, E. Martin, R. Martin-Solis[8], P. Massmann, G. Matthews, H. McBryan, G. McCracken[7], P. Meriguet, P. Miele, S.F. Mills, P. Millward, E. Minardi[16], R. Mohanti[17], P.L. Mondino, A. Montvai[3], P. Morgan, H. Morsi, G. Murphy, F. Nave[27], S. Neudatchin[23], G. Newbert, M. Newman, P. Nielsen, P. Noll, W. Obert, D. O'Brien, J. O'Rourke, R. Ostrom, M. Ottaviani, S. Papastergiou, D. Pasini, B. Patel, A. Peacock, N. Peacock[7], R.J.M. Pearce, D. Pearson[12], J.F. Peng[26], R. Pepe de Silva, G. Perinic, C. Perry, M.A. Pick, J. Plancoulaine, J-P. Poffé, R. Pohlchen, F. Porcelli, L. Porte[19], R. Prentice, S. Puppin, S. Putvinskii[23], G. Radford[9], T. Raimondi, M.C. Ramos de Andrade, M. Rapisarda[29], P-H. Rebut, R. Reichle, S. Richards, E. Righi, F. Rimini, A. Rolfe, R.T. Ross, L. Rossi, R. Russ, H.C. Sack, G. Sadler, G. Saibene, J.L. Salanave, G. Sanazzaro, A. Santagiustina, R. Sartori, C. Sborchia, P. Schild, M. Schmid, G. Schmidt[6], H. Schroepf, B. Schunke, S.M. Scott, A. Sibley, R. Simonini, A.C.C. Sips, P. Smeulders, R. Smith, M. Stamp, P. Stangeby[20], D.F. Start, C.A. Steed, D. Stork, P.E. Stott, P. Stubberfield, D. Summers, H. Summers[19], L. Svensson, J.A. Tagle[21], A. Tanga, A. Taroni, C. Terella, A. Tesini, P.R. Thomas, E. Thompson, K. Thomsen, P. Trevalion, B. Tubbing, F. Tibone, H. van der Beken, G. Vlases, M. von Hellermann, T. Wade, C. Walker, D. Ward, M.L. Watkins, M.J. Watson, S. Weber[10], J. Wesson, T.J. Wijnands, J. Wilks, D. Wilson, T. Winkel, R. Wolf, D. Wong, C. Woodward, M. Wykes, I.D. Young, L. Zannelli, A. Zolfaghari[28], G. Zullo, W. Zwingmann.

PERMANENT ADDRESSES

1. UKAEA, Harwell, Didcot, Oxon, UK.
2. University of Leicester, Leicester, UK.
3. Central Research Institute for Physics, Budapest, Hungary.
4. University of Essex, Colchester, UK.
5. University of Birmingham, Birmingham, UK.
6. Princeton Plasma Physics Laboratory, New Jersey, USA.
7. UKAEA Culham Laboratory, Abingdon, Oxon, UK.
8. Universidad Complutense de Madrid, Spain.
9. Institute of Mathematics, University of Oxford, UK.
10. Freien Universität, Berlin, F.R.G.
11. Royal Institute of Technology, Stockholm, Sweden.
12. Imperial College, University of London, UK.
13. Max Planck Institut für Plasmaphysik, Garching, FRG.
14. Risø National Laboratory, Denmark.
15. FOM Instituut voor Plasmafysica, Nieuwegein, The Netherlands.
16. Dipartimento di Fisica, University of Milan, Milano, Italy.
17. North Carolina State University, Raleigh, NC, USA
18. National Institute for Fusion Science, Nagoya, Japan.
19. University of Strathclyde, 107 Rottenrow, Glasgow, UK.
20. Institute for Aerospace Studies, University of Toronto, Ontario, Canada.
21. CIEMAT, Madrid, Spain.
22. Institute for Nuclear Studies, Otwock-Swierk, Poland.
23. Kurchatov Institute of Atomic Energy, Moscow, USSR
24. Queens University, Belfast, UK.
25. Keldysh Institute of Applied Mathematics, Moscow, USSR.
26. Institute of Plasma Physics, Academica Sinica, Hefei, P. R. China.
27. LNETI, Savacem, Portugal.
28. Plasma Fusion Center, M.I.T., Boston, USA.
29. ENEA, Frascati, Italy.

At 1st July, 1992